Flexural strengthening of large-scale reinforced concrete beams using near-surface-mounted self-prestressed iron-based shape-memory alloy strips

Raafat El-Hacha and Hothifa Rojob

- An experimental program was conducted to investigate the performance of large-scale reinforced concrete beams strengthened with near-surface-mounted iron-based shape-memory alloy strips.
- The results revealed the effectiveness of the strengthening technique in enhancing the flexural performance of the strengthened beams at service and ultimate load conditions.
- Comparison with carbon-fiber-reinforced-polymer-strengthened beams revealed the superiority of the near-surface-mounted iron-based shape-memory alloy in maintaining the ductile behavior of the strengthened beams.

Several reports paint a bleak picture of the condition of North America's infrastructure. The 2016 Canadian Infrastructure Report Card[1] says that one third of the municipal infrastructure is in fair, poor, or very poor condition, and the replacement value of the bridges alone was estimated to be CAD 20.8 billion. The 2017 Report Card for America's Infrastructure[2] says that 9.1% of U.S. bridges are rated structurally deficient. To eliminate the deficient bridge backlog in the United States by 2028, the Federal Highway Administration estimates that they need to invest USD 20.5 billion annually.[3] In light of these facts, researchers have been looking for practical, efficient, and economical retrofitting and strengthening techniques to repair deteriorated structures.

Shape-memory alloy

Recently, a new class of smart materials called shape-memory alloys (SMAs), in the form of wires and bars, has been attracting researchers from different fields. SMAs are a unique class of metallic alloys that have the ability to undergo large deformations (up to 8%) and return to their original shape through stress removal, that is, unloading (superelasticity effect) or heating (shape-memory effect). These unique properties of SMAs are a direct result of temperature- or stress-induced phase transformation of the material between its crystallographic phases: the martensite (low temperature) phase and austenite (high temperature) phase. The bold-centered-cubic structure that is the parent phase is called the austenite phase, and the product phase is known as the martensite phase.

SMA materials have the ability to transform from the martensite phase to the austenite phase by a process called reverse martensite transformation. The superelasticity effect occurs when an external stress is applied to the material at a constant temperature state, causing the material to undergo phase transformation from austenite to martensite. Upon unloading the applied stress, a diffusionless solid state reverse transformation occurs from the martensite to the austenite phase and the initial shape of the material is reformed.

The shape-memory effect occurs when an SMA material in the detwinned martensite phase is heated above the activation temperature, which results in a more thermodynamically stable austenite phase.[4] This process is associated with a macroscopic shape change.

Figure A1 (for appendix figures, go to https://pci.org/2018-11-12-Appx) shows a temperature-stress phase diagram of the shape-memory effect process of iron-based SMA (Fe-SMA) material from points 1 to 4. The parent austenite phase is first loaded to form the stress-induced detwinned martensite phase at a temperature above the martensite start temperature M_s, where a single variant dominates.

The detwinning process starts at a stress level called the detwinning start σ_s and finishes at a stress level called the detwinning finish σ_f, causing macroscopic permanent deformation. The martensite remains detwinned after unloading. In the absence of stress and upon application of heat above the austenite start temperature A_s, the detwinned martensite material starts to recover the permanent deformations and completely transforms to the parent austenite phase at the austenite finish temperature A_f. More details about martensite transformation in Fe-SMA can be found in the references.[4–6]

The recent development of Fe-SMA offers new possibilities for the rehabilitation of structures.[7–10] Fe-SMA is relatively inexpensive compared with traditional nickel titanium SMA (NiTi-SMA), which makes it more suitable for large-scale structural engineering applications.[5,7] The use of NiTi-SMA in structural engineering applications has been limited to small-scale members and not adopted in practical application due to two main challenges: the relatively high cost of the material and production methods and its thermal instability when exposed to ambient temperature, which can result in reverse transformation.[9,10]

In addition to their superelasticity and resistance to corrosion and fatigue, SMAs are mainly characterized by the shape-memory effect property that is the result of their unique thermomechanical properties.[11,12] This makes them attractive materials for various civil engineering applications, such as braces, base isolators, damage repair devices, and bridge restrainers.[13–15] Their unique properties also make them a suitable candidate for seismic retrofitting concrete structures.

Recent progress

The shape-memory effect of SMAs makes them suitable for external prestressing to strengthen reinforced concrete beams. A review of the literature revealed no real-life applications of NiTi SMAs for flexural strengthening of reinforced concrete beams. This is due to the relatively high cost of NiTi-SMAs compared with currently used materials, such as fiber-reinforced polymers (FRPs).

To eliminate the use of hydraulic jacks to prestress FRP reinforcements for the flexural strengthening of reinforced concrete beams, El-Hacha and Hadiseraji[16,17] proposed an innovative application of prestrained NiTi-SMA bars to act as actuators connected to end anchors attached to externally bonded FRP sheets and to near-surface-mounted FRP strips. The prestressing force induced in the FRP was applied by activating the SMA bar through heating above its activation temperature. This active prestressed strengthening technique provides stresses in the beam that partially counteract the stresses induced in the beam due to applied gravity loads. However, the recent development of corrosion-resistant Fe-SMA (through the addition of Cr and Ni)—with its considerably lower cost, higher recovery stress, and a larger thermal hysteresis that prevents reverse transformation—has made this new material the choice for structural engineering applications.[4,6,9,18]

If a prestrained SMA material is heated above the activation temperature, the heating triggers the shape-memory phenomenon, causing the material to recover part of the induced strain. However, if the edges of the SMA material are restrained, stress will develop in the material instead of shape recovery. This stress can be used for structural engineering applications.

The first reported attempt to use Fe-SMA bars in structural rehabilitation was by Soroushian et al.[19] Soroushian used a total of 24 Fe-SMA bars with 10.4 mm (0.41 in.) diameters for external post-tensioning to strengthen a bridge girder for shear. The bars were anchored to the sides of concrete beams inclined at 35 degrees. The bars generated 120 MPa (17 ksi) of stress when heated with an electric resistance heating system of 1000 A, causing a 40% reduction in crack widths and restoring the shear strength of the girder.

To investigate the feasibility of Fe-SMA strips for prestressed strengthening of reinforced concrete structures, Czaderski et al.[8] used Fe-SMA strips to apply prestressing force to nine small concrete bars. The authors concluded that Fe-SMA can be used as a strengthening material for reinforced concrete beams using the near-surface-mounted technique.

Recently, Rojob and El-Hacha[6] used smooth Fe-SMA bars for flexural strengthening of 1.8 m (5.9 ft) long reinforced concrete beams using the near-surface-mounted technique. The bars were placed in a precut groove in the tension side of the beam and anchored at both ends. Using the same strengthening technique and the same beam configuration, Rojob and El-Hacha have also studied the performance of Fe-SMA–

strengthened reinforced concrete beams under severe freezing and thawing exposure[20] and under fatigue loading.[21]

Shahverdi et al.[22] used Fe-SMA ribbed strips as near-surface-mounted reinforcements for the flexural strengthening of 2.0 m (6.6 ft) long reinforced concrete beams. The strips were activated using electrical current after filling the pre-cut grooves with cement-based grout. Shahverdi et al.[23] also strengthened reinforced concrete beams with the same configurations as the previous beams but with the Fe-SMA bars embedded in a shotcrete layer at the tension face of the beam.

The studies by Rojob and El-Hacha and Shahverdi et al. revealed significant enhancement of the flexural capacity of the strengthened beams at service and ultimate load conditions compared with the unstrengthened control beams.

The objective of the study presented in this paper was to investigate the flexural performance of large-scale beams strengthened with near-surface-mounted Fe-SMA strips by utilizing the SME phenomenon. Four beams were tested: one control beam, one beam strengthened with nonactivated Fe-SMA strips, and two beams strengthened with a different number of activated Fe-SMA strips. The results were compared with similar beams found in the literature strengthened with prestressed, near-surface-mounted carbon-fiber-reinforced-polymer (CFRP) bars. The results revealed the effectiveness of near-surface-mounted Fe-SMA in strengthening large-scale beams.

Experimental program

Test specimens and loading setup

Four large-scale reinforced concrete beams were tested monotonically to failure under four-point bending. The four beams consisted of a control beam B-C and three beams strengthened with near-surface-mounted Fe-SMA strips. Beam B-SMA-0 was strengthened with five Fe-SMA strips without activation, while beams B-SMA-1 and B-SMA-2 were strengthened with five and seven activated Fe-SMA strips, respectively.

The load was applied in a displacement-controlled mode using a 250 kN (56 kip) actuator. The displacement rate was selected as 1 mm (0.04 in.) per minute until the yielding load and then increased to 3 mm (0.1 in.) per minute until failure.

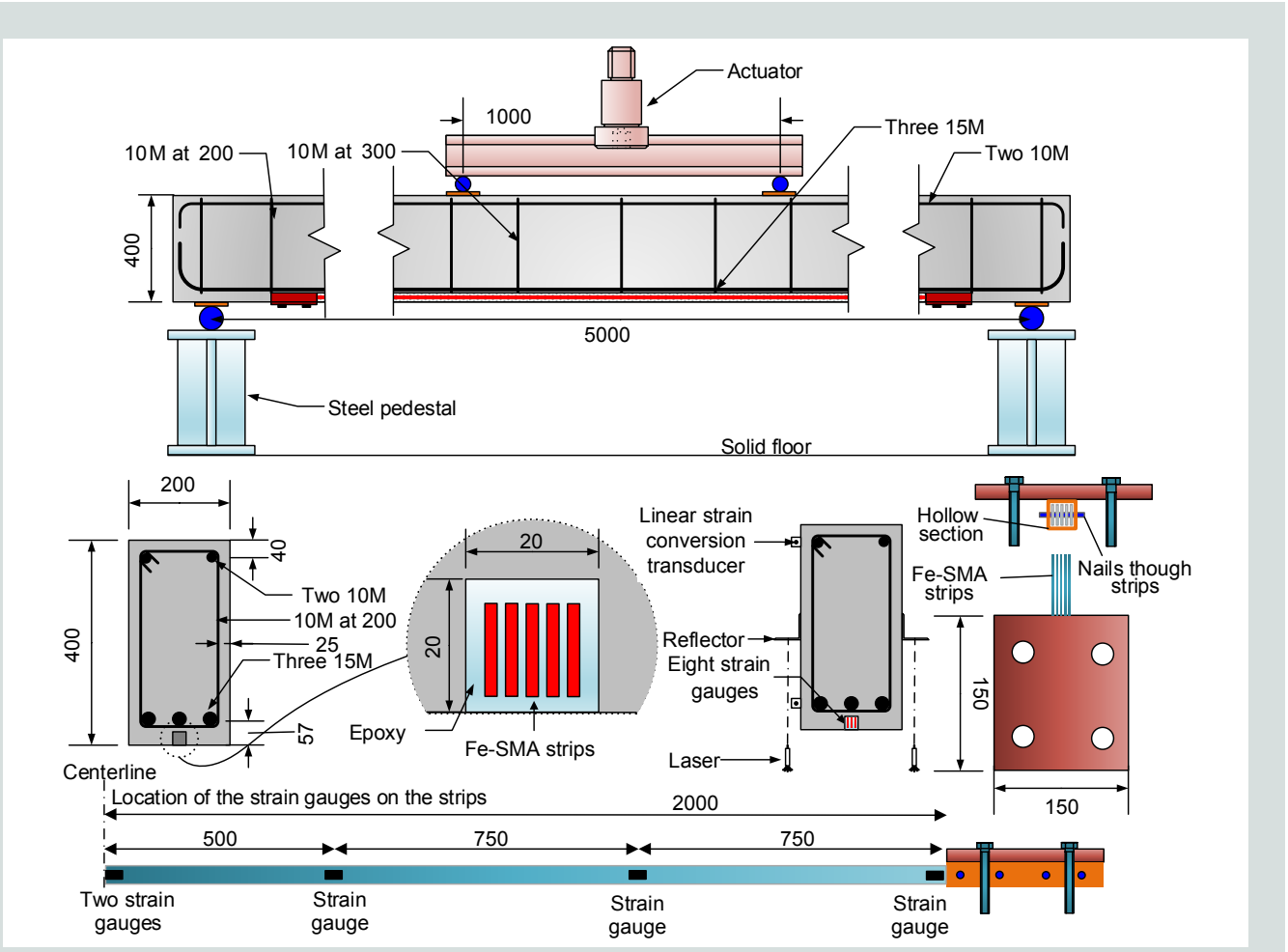

Figure 1. Geometric details of a typical beam. Note: All dimensions are in millimeters. Fe-SMA = iron-based shape-memory alloy. 10M = no. 3; 15M = no. 5; 1 mm = 0.0394 in.

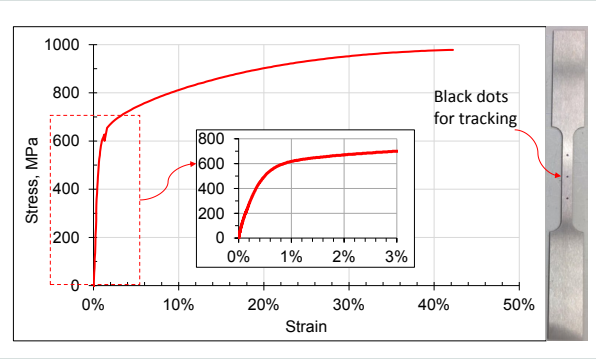

Figure 2. Stress-strain behavior of the iron-based shape-memory alloy strips and the specimen used for the tensile testing. Note: 1 MPa = 0.145 ksi.

The span of the beams was 5.0 m (16 ft) (center to center between the supports) with a cross section of 200 × 400 mm (8 × 16 in.). **Figure 1** shows a typical schematic drawing of a reinforced concrete beam along with instrumentation details. The beams were reinforced with three 15M (no. 5) steel bars in the tension side and two 10M (no. 3) steel bars in the compression side, with a total cross-sectional area of 600 mm^2 (0.9 $in.^2$) and 200 mm^2 (0.3 $in.^2$), respectively. Two-legged 10M steel stirrups were uniformly spaced at 300 mm (12 in.) in the constant moment region and 200 mm (8 in.) elsewhere. The control beam was designed according to CSA 23.3-04[24] as an underreinforced beam; that is, failure occurs by crushing of the concrete after yielding of the steel reinforcements.

The beams were instrumented with four strain gauges mounted on the tension and compression steel at the midspan (two for each). The midspan deflection was measured using two laser transducers on each side of the beam. Two linear strain conversion transducers were mounted at the level on the tension and compression steel at the midspan to measure the strain in the concrete. The Fe-SMA strips in beam B-SMA-0 were instrumented with eight strain gauges along the length of the strips (Fig. 1). The Fe-SMA strips in the other beams were not instrumented with strain gauges because the activation of the strips through heating would have damaged the strain gauges.

Steel and concrete material properties

The yield strength and modulus of elasticity of the 15M (no. 5) bars were 410 ± 3.2 MPa (59.5 ± 0.46 ksi) and 175.2 ± 6.3 GPa (25,410 ± 913 ksi), respectively, and 474.7 ± 1.2 MPa (68.85 ± 0.17 ksi) and 177.7 ± 3.8 GPa (25,770 ± 550 ksi) for the 10M (no. 3) bars. The results were based on unidirectional tensile testing of three specimens according to ASTM A370-14.[25] Two batches of concrete were used to cast the beams, one batch to cast beams B-C and B-SMA-0 and the other to cast beams B-SMA-1 and B-SMA-2. The specified concrete compressive strength was 40 MPa (5.8 ksi). **Table A1** shows the details of the concrete compressive strength at 28 days and on the day of testing. Three concrete specimens were used for each test.

Fe-SMA material

Material characteristics The stress-strain behavior of the Fe-SMA strips was determined in accordance with ASTM A370.[25] Because the ultimate strain of such material is relatively high and the available strain gauges cannot read more than 3% to 5% strain, the digital image correlation technique (DICT) was employed to measure the development of strain during tensile loading. Solid black dots were put on the surface of the dog-bone-shaped specimens as a tracking points for the DICT (**Fig. 2**). Figure 2 shows the stress-strain behavior of the Fe-SMA material. The behavior of the Fe-SMA strips can be divided into three approximately trilinear stages: the initial high-stiffness stage of about 116 GPa (16,800 ksi) up to a stress level of 400 MPa (58 ksi), followed by the intermediate-stiffness stage of 38 GPa (5500 ksi) between stress levels of 400 to 600 MPa (87 ksi), and finally the low-stiffness stage of 1 GPa (145 ksi) from 600 MPa (87 ksi) stress until the failure.

Preparation of the Fe-SMA strips Strips were cut from 5000 mm (200 in.) long, 100 mm (4 in.) wide, 1.5 mm (0.06 in.) thick Fe-SMA sheets. The sheets were cut into 15.8 mm (0.622 in.) wide strips using a waterjet cutting machine. Waterjet cutting was used instead of laser cutting because the heat generated by laser cutting would have altered the material characteristics. **Figure A2** shows the Fe-SMA sheets and strips.

Before being anchored in the beams, the Fe-SMA strips were strained to about 3%, as recommended by the manufacturer. This initial strain value is the optimum value that results in the highest recovery stress upon heating. A reaction frame was built to apply the initial strain to the strips (**Fig. A3**). The strain was applied to groups of three strips gripped between two thick steel plates pre-welded to a bar. The load was applied through a hydraulic jack that pulled the bar. To confirm the uniformity of the strain during loading, the strain was measured at different locations along the strips. **Figure A4** compares the load and strain at different locations during the application of the initial strain. The drop indicated in the curve is due to the slip that occurred at one of the end gripping tools. The load was applied again after the slippage issue was fixed. The strain distribution (Fig. A4) confirms the uniformity of the strain distribution along the Fe-SMA strips with a slightly higher strain at the midspan of the center strip (strain gauge 2).

Strengthening procedure

Anchorage system After the initial strain was applied to the Fe-SMA strips, the strips were inserted into specially designed end anchors. Five steel nails with diameters of 3 mm (0.1 in.) were driven through the strips. The size and number of steel nails were proportioned to provide sufficient anchorage to the Fe-SMA strips during the activation process. The tubes were then filled with epoxy adhesive. The strips were bent at the ends of the steel tube and welded to the sides of the tube (**Fig. A5**). Spacers were used temporarily to keep the Fe-SMA strips apart until the epoxy adhesive had cured.

The space between the Fe-SMA strips was needed for the activation process because heating tapes were to be inserted between the strips.

To confirm the adequacy of the anchorage system, a separate specimen was prepared and tested under unidirectional tensile loading until failure (**Fig. A6**). **Figure A7** compares the tensile load and strain measured in the Fe-SMA strips. The strips failed by tensile rupture of the net area at the location of the first nail (Fig. A6) at an ultimate load of 80 kN (18 kip). Because the amount of the prestressing force generated in the Fe-SMA strips upon heating when anchored in the beams was estimated to be 32.5 kN (7.31 kip), the anchor was considered adequate to hold that force without failure.

The Fe-SMA strips with the end anchors were placed in a precut groove in the tension side of the reinforced concrete beams. The steel plates were then anchored to the soffit of the beams using steel expansion anchors (**Fig. A8**). Before driving the expansion anchors into the holes, the holes were filled with epoxy adhesive.

Activation of the Fe-SMA strips To activate the prestrained Fe-SMA strips, the strips were heated above the activation temperature of 150°C (302°F). Flexible heating tape was put between the strips (**Fig. A9**). Three thermocouples installed on Fe-SMA strips were used to monitor the temperature during the heating process at different locations. During heating, the strain in the tension steel was reported as an indirect way of monitoring the development of the prestressing force in the near-surface-mounted Fe-SMA strips.

Grouting After the Fe-SMA strips cooled to room temperature, the grooves were filled with paste adhesive. A spatula was used to force the paste between the strips (**Fig. A10**).

Results and discussion

Prestressing stage

The prestressing force generated in the Fe-SMA strips was estimated based on the strain developed in the tension steel during the activation process. **Figure 3** shows the change in strain in the tension steel (compression strain due to the prestressing force, which was used as positive strain) in beams B-SMA-1 and B-SMA-2. The slight reduction in the strain at the beginning of the activation process was due to the thermal expansion effect. At a temperature of 110°C (230°F), the strain started to increase; that is, the prestressing force started to develop in the Fe-SMA strips. The strain continued to increase at a low rate until the end of the heating stage (at a temperature of 155°C [311°F]). During the cooling stage, the prestressing force continued to increase due to the shape transformation and the removal of the thermal expansion effect. The strain dropped slightly at room temperature due to a partial reverse transformation from the austenite to martensite phases. In beam B-SMA-2, the strips were heated in two stages because there was not enough heating tape to heat the seven strips simultaneously. Figure 3 shows the point at which the last set of strips was heated. The difference between the compression strain at the beginning and end of the heating-cooling cycle is the amount of strain that corresponds to the prestressing force. To estimate the prestressing force P generated in the Fe-SMA strips, the following linear elastic analysis was used:

$$P = \frac{\varepsilon_c E_c}{\left(\frac{1}{A_g} + \frac{ey}{I_g}\right)}$$

where

ε_c = strain in the concrete at the level of the tension steel (taken from the readings of the strain gauges attached to the tension steel at the midspan, assuming strain compatibility between the steel and the concrete)

E_c = modulus of elasticity of the concrete = $4500\sqrt{f'_c}$, in accordance with CSA A23.1-04[21]

f'_c = compressive strength of concrete

A_g = gross area of the beam cross section

e = eccentricity of the Fe-SMA strips = 192 mm (7.56 in.)

y = distance from the center of gravity of the tension steel to the center of gravity of the beam's cross section = 150 mm (6 in.)

I_g = moment of inertia of the beam cross section

The prestressing forces were calculated to be 31.7 and 49 kN (7.12 and 11 kip) for beams B-SMA-1 and B-SMA-2, respectively. These prestressing forces correspond to stress levels of 268 and 295 MPa (38.9 and 42.8 ksi) in the Fe-SMA strips

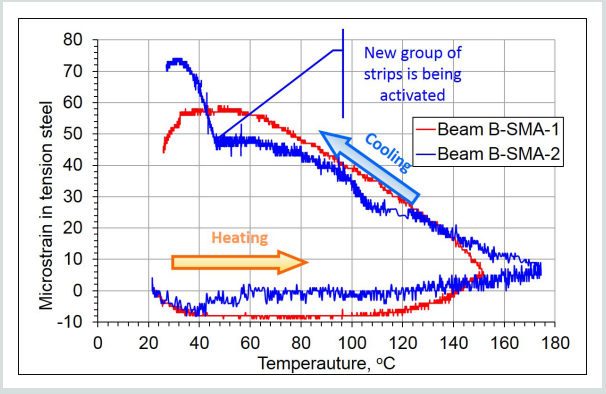

Figure 3. The change of strain (the compression strain was considered positive) over temperature in the tension steel during the activation process of the iron-based shape-memory alloy strip in beams B-SMA-1 and B-SMA-2. Note: SMA = shape-memory alloy. °C = (°F – 32)/1.8.

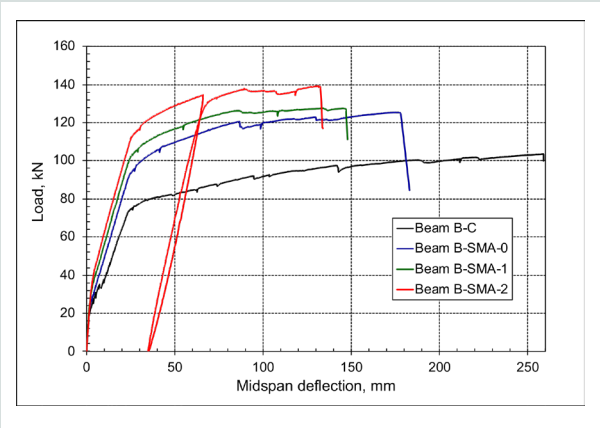

Figure 4. The load versus the midspan deflection curve of all beams. Note: 1 mm = 0.0394 in.; 1 kN = 0.225 kip.

in beams B-SMA-1 and B-SMA-2, respectively. The amount of recovery stress obtained from the activation process was comparable to the recovery stress value of 274 MPa (39.7 ksi) obtained by the shape-memory effect test, as reported by the manufacturer. There were no signs of anchorage setting during the activation process, which proves the efficiency of the end anchors. Anchorage setting would have resulted in a sudden drop in the compression strain in the tension steel, as reported by Rojob and El-Hacha.[6]

Loading stage

Load deflection response As indicated in Fig. 1, all beams were loaded monotonically in a four-point bending setup until failure. **Figure 4** compares the load and midspan deflection curve of all beams. Beam B-SMA-2 was unloaded at 136.5 kN (30.69 kip) due to a technical issue and then loaded again until failure. The control beam failed by crushing of the concrete after yielding of the steel reinforcement. Similarly, the strengthened beams failed by crushing of concrete after yielding of the steel reinforcement and after the Fe-SMA strips entered the low-stiffness stage of its stress-strain behavior. (This stage of Fe-SMA behavior will be called the yielding stage from now on.)

Effectiveness of the strengthening technique **Table 1** summarizes the test results for all beams. At service conditions, the beams strengthened with activated Fe-SMA strips, B-SMA-1 and B-SMA-2, showed 29% and 59% increases in the cracking load and 40% and 53% increases in the yielding load, respectively, compared with beam B-C. The nonactivated beam B-SMA-0 showed a 25% increase in cracking and yielding loads. At ultimate conditions, the ultimate load capacities of beams B-SMA-0, B-SMA-1, and B-SMA-2 increased 21%, 23%, and 34%, respectively, compared with the control beam. More important, due to the yielding nature of the Fe-SMA strips, the strengthened beams exhibited a large deflection after the yielding load until the crushing of concrete. The reduction in the ultimate deflection of beam B-SMA-1 with five activated Fe-SMA strips, compared with beam B-SMA-0 with five nonactivated Fe-SMA strips, was about 16%. In other words, activating the Fe-SMA strips did not cause a significant reduction in the ductility of the beam. Furthermore, the total dissipated energy—calculated as the area under the load deflection curve until the crushing of the concrete—in beams B-SMA-1 and B-SMA-2 was reduced by 16% and 18%, respectively, over the nonactivated beam B-SMA-0 and 29% and 31% over the control beam B-C.

Strain distribution **Figure A11** shows the strain distribution across the depth of the beams at the midspan section at cracking, yielding, and ultimate loads. The strain distribution is linear across the depth of the beams at all loading stages. The strain in the Fe-SMA strips at the midspan was only reported for beam B-SMA-0 because no strain gauges were used in the other beams, as mentioned previously. The strain in the Fe-SMA strips was taken as the average of the strains measured by the three strain gauges in the constant moment region. At the cracking and yielding loads, the strain distribution was linear in beam B-SMA-0, which indicates full compatibility between the Fe-SMA strips and the surrounding grout. However, at the ultimate load, the strain in the Fe-SMA strips was smaller than

Table 1. Summary of the test results

Test parameter	B-C	B-SMA-0	Δ, %	B-SMA-1	Δ, %	B-SMA-2	Δ, %
Cracking load P_{cr}, kN	19.6	24.5	25	25.2	29	31.2	59
Yielding load P_y, kN	73.5	92	25	103	40	112.6	53
Ultimate load P_u, kN	103.5	124.8	21	127.3	23	138.9	34
Deflection at yield Δ_y, mm	23.8	24.6	3	25.6	8	25	5
Deflection at ultimate Δ_u, mm	258.0	175.0	-32	146.5	-43	132	-49
Ductility index Δ_u/Δ_y	10.8	7.1	-34	5.7	-47	5.3	-51
Energy dissipated,* kN-mm x 10^3	23.2	19.4	-16	16.5	-29	15.9	-31

Note: SMA = shape-memory alloy; Δ = difference. 1 mm = 0.0394 in.; 1 kN = 0.225 kip.

*Calculated as the area under the load deflection curve up to the ultimate load.

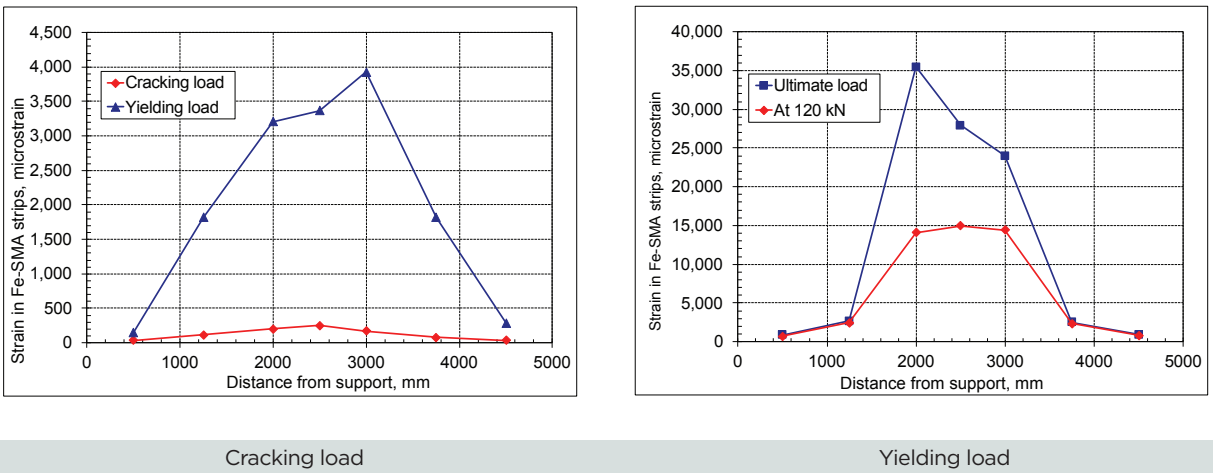

Figure 5. Strain profile along the Fe-SMA strips in beam B-SMA-0. Note: Fe-SMA = iron-based shape-memory alloy; SMA = shape-memory alloy. 1 mm = 0.0394 in.; 1 kN = 0.225 kip.

the tension-steel strain, which indicates that slippage occurred between the Fe-SMA strips and the surrounding grout.

Bond characteristics There were no visible signs of separation or cracking on the paste adhesive in any of the strengthened beams. **Figure 5** shows the strain profile along the Fe-SMA strips in beam B-SMA-0. Lower strains near the anchors indicate that the bond was able to transfer the load carried by the Fe-SMA strips to the concrete. The strain in the constant moment region was relatively constant up to the load of 120 kN (27 kip), equivalent to a 100 mm (4 in.) midspan deflection, after which the strain to the left of the midspan became greater than the strain to the right, which indicates debonding in that localized region. **Figure 6** shows the strain in the Fe-SMA strips and in the tension steel at the midspan of beam B-SMA-0. The strain in the Fe-SMA strips was higher than that in the steel until the yielding load, which indicates debonding between the Fe-SMA and the grout at the midspan.

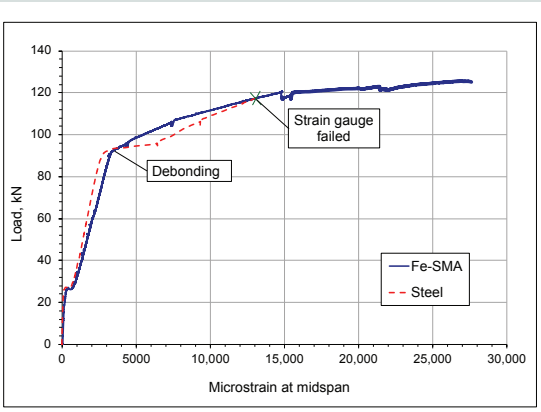

Figure 6. The development of strain over load in Fe-SMA strips and tension steel at the midspan of beam B-SMA-0. Note: Fe-SMA = iron-based shape-memory alloy; SMA = shape-memory alloy. 1 kN = 0.225 kip.

Cracking pattern Typical flexural cracking patterns were exhibited by all beams (**Fig. 7**). The cracks were distributed uniformly, similar to the control beam B-C. No cracks were observed around the end anchors, except for beam B-SMA-2, where a crack was observed around the anchors at a load of 134 kN (30.1 kip), which was close to the ultimate load of 138.9 kN (31.23 kip).

Comparison with prestressed, near-surface-mounted CFRP strengthening

The performances of the SMA-strengthened beams, B-SMA-1 and B-SMA-2, were compared with similar beams strengthened with near-surface-mounted, prestressed CFRP bars tested by El-Hacha and Gaafar.[26] The beams strengthened with CFRP were designated CFRP-20 and CFRP-40, where 20 and 40 refer to the prestressing levels as percentages of the ultimate tensile strength of the CFRP bars. El-Hacha and Gaafar selected the 40% prestressing level as the optimum prestressing level that results in enhancing the flexural capacity of the beam with sufficient ductility. The amount of prestressing forces in beams CFRP-20 and CFRP-40 were 27.4 kN (6.16 kip) and 52.6 kN (11.8 kip), respectively.[26] The prestressing forces applied to the CFRP bars were comparable to the prestressing forces developed in the Fe-SMA strips in beams B-SMA-1 and B-SMA-2: 31.7 kN (7.12 kip) and 49 kN (11 kip), respectively. **Figure 8** shows the load deflection curves of the CFRP-strengthened and SMA-strengthened beams.

Table A2 shows a comparison between the CFRP-strengthened and SMA-strengthened beams. At the service load conditions, the SMA-strengthened and CFRP-strengthened beams exhibited comparable performances. At ultimate conditions, beams CFRP-20 and CFRP-40 exhibited slight-

Figure 7. Crack patterns in all beams.

ly higher ultimate capacities than beams B-SMA-1 and B-SMA-2, with 11% and 2% higher load capacities, respectively. However, the increase in the ultimate load capacities of the CFRP-strengthened beams significantly compromised the beams' ductility. Furthermore, El-Hacha and Gaafar[26] reported that beams CFRP-20 and CFRP-40 failed in a brittle mode by sudden rupture of the near-surface-mounted CFRP bars. The ductility indices of beams CFRP-20 and CFRP-40 were 71% and 90% less than for beams B-SMA-1 and B-SMA-2, respectively. In summary, the SMA-strengthened beams maintained service and ultimate load capacities comparable to those of the CFRP-strengthened beams while not significantly compromising the ductility of the beams or changing their failure mode. The SMA-strengthened beams failed in ductile mode, similar to the failure of the underreinforced beams.

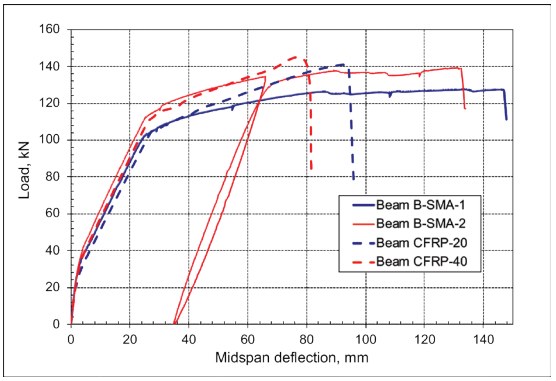

Figure 8. Load deflection curves of the CFRP-strengthened beams and SMA-strengthened beams. Note: CFRP = carbon-fiber-reinforced polymer; SMA = shape-memory alloy. 1 mm = 0.0394 in.; 1 kN = 0.225 kip.

Conclusion

A self-prestressing technique using near-surface-mounted Fe-SMA strips was proved to be an efficient technique to enhance the flexural capacity of reinforced concrete beams without the need for sophisticated on-site jacking tools. Four large-scale reinforced concrete beams were tested in total, three of which were strengthened with Fe-SMA strips. The following conclusions were drawn:

- The beams strengthened with activated near-surface-mounted Fe-SMA strips experienced an enhancement in flexural performance at service and ultimate load conditions.
- The strengthened beams failed by crushing of concrete after yielding of the steel reinforcement and the Fe-SMA strips, similar to the unstrengthened beam. The ductility of the strengthened beams was comparable to that of the unstrengthened beam due to the yielding nature of the Fe-SMA strips.
- The end anchors designed in the current research were able to transfer the load during the activation and the loading stages with no signs of anchorage settings. The prestressing forces resulting from the activation of the Fe-SMA strips were close to the values estimated by the manufacturer.
- The bond between the Fe-SMA strips and the grout was strong until the yielding load, where a localized debonding occurred in the midspan. There were no signs of longitudinal cracks in the grout in any of the strengthened beams.

- A comparison between near-surface-mounted, prestressed CFRP-strengthened beams and self-prestressed, near-surface-mounted SMA-strengthened beams with comparable prestressing forces revealed that the two systems perform comparably at service load conditions. While the CFRP-strengthened beams attained a slightly higher ultimate strength than the SMA-strengthened beams, the CFRP-strengthened beams experienced a significant reduction in ductility and failed by a sudden rupture of the CFRP bars. In contrast, the SMA-strengthened beams maintained a ductile behavior and the failure mode was similar to that of the underreinforced beams.

In summary, the self-prestressing, near-surface-mounted Fe-SMA strengthening system is a promising technique in the field of rehabilitation of existing structures because of its ease of application, relatively inexpensive material, and yielding nature that ensures that the failure mode of the underreinforced reinforced concrete beams will be maintained.

Acknowledgments

The authors would like to acknowledge the University of Calgary and the Natural Sciences and Engineering Research Council of Canada for their financial support. The authors would also like to thank the Swiss Federal Laboratories for Materials Science and Technology and Re-fer Strengthening Solutions for providing the Fe-SMA sheets, Sika for providing the epoxy and the grout material, Lafarge Canada for supplying the concrete, and Hughes Brothers for providing the CFRP bars. Further, the authors would like to acknowledge the laboratory technicians in the structural engineering lab at the University of Calgary for their help in conducting the experiments.

References

1. CIRC (Canadian Infrastructure Report Card) Project Steering Committee. 2016. *Informing the Future: The Canadian Infrastructure Report Card.* http://canadianinfrastructure.ca/downloads/Canadian_Infrastructure_Report_2016.pdf.

2. ASCE (American Society of Civil Engineers). 2017. "2017 Report Card for America's Infrastructure." https://www.infrastructurereportcard.org/.

3. FHWA (Federal Highway Administration). 2013. "Deficient Bridges by State and Highway System 2013." http://www.fhwa.dot.gov/bridge/nbi/no10/defbr13.cfm.

4. DoITPoMS (Dissemination of IT for the Promotion of Materials Science). 2009. "Superelasticity and Shape Memory Alloys." DoITPoMS teaching and learning package. http://www.doitpoms.ac.uk/tlplib/superelasticity/index.php.

5. Cladera, A., B. Weber, C. Leinenbach, C. Czaderski, M. Shahverdi, and M. Motavalli. 2014. "Iron-Based Shape Memory Alloys for Civil Engineering Structures: An Overview." *Construction and Building Materials* 63: 281–293.

6. Rojob, H., and R. El-Hacha. 2016. "Self-prestressing Using Iron-Based Shape Memory Alloy for Flexural Strengthening of Reinforced Concrete Beams." *ACI Structural Journal* 114 (2): 523–532.

7. Awaji. 2014. "Shape Memory Alloy." http://www.awaji-m.jp/english/r_and_d/about.html.

8. Czaderski, C., M. Shahverdi, R. Bronnimann, C. Leinenbach, and M. Motavalli. 2014. "Feasibility of Iron-Based Shape Memory Alloy Strips for Prestressed Strengthening of Concrete Structures." *Construction and Building Materials* 56: 94–105.

9. Dong, Z., U. Klotz, C. Leinenbach, A. Bergamini, C. Czaderski, and M. Motavalli. 2009. "A Novel Fe-Mn-Si Shape Memory Alloy with Improved Shape Recovery Properties by VC Precipitation." *Advanced Engineering Materials* 11 (1): 40–44.

10. Li, K., Z. Dong, Y. Liu, and L. Zhang. 2013. "A Newly Developed Fe-Based Shape Memory Alloy Suitable for Smart Civil Engineering." *Smart Materials and Structures* 22 (4): 1–7.

11. Lagoudas, D. C. 2008. *Shape Memory Alloys: Modeling and Engineering Applications*. New York, NY: Springer Science.

12. Cismasiu, C. 2010. *Shape Memory Alloys*. Rijeka, Croatia: Sciyo.

13. Cardone, D., M. Dolcw, C. Ponzo, and E. Coelho. 2004. "Experimental Behaviour of R/C Frames Retrofitted with Dissipating and Re-Centring Braces." *Journal of Earthquake Engineering* 8 (3): 361–396.

14. Ocel, J., R. DesRoches, R. T. Leon, W. G. Hess, R. Krumme, J. R. Hayes, and S. Sweeney. 2004. "Steel Beam-Column Connections Using Shape Memory Alloys." *Journal of Structural Engineering*, 130 (5): 732–740.

15. Shin, M., and B. Andrawes. 2010. "Experimental Investigation of Actively Confined Concrete Using Shape Memory Alloys." *Engineering Structures* 32 (3): 656–664.

16. Hadiseraji, M., and R. El-Hacha. 2014. "Flexural Strengthening of Reinforced Concrete Beams with Prestressed Externally Bonded CFRP Sheets." In *Concrete Solutions, 5th International Conference on Concrete Repair Proceedings, September 1–3, 2014, Belfast, Northern Ireland, UK*. Boca Raton, FL: CRC Press.

17. Hadiseraji, M., and R. El-Hacha. 2014. "Strengthening RC Beams with Prestressed Near-Surface Mounted CFRP Strip." In *7th International Conference on FRP Composites in Civil Engineering Proceedings, August 20–22, 2014, Vancouver, BC, Canada*. Calgary, AB, Canada: University of Calgary.

18. Rojob, H., and R. El-Hacha. 2015. "Numerical Investigation of the Flexural Performance of RC Beam Strengthened with Iron-Based Shape Memory Alloy Bar." In *27th Biennial National Conference of the Concrete Institute of Australia in conjunction with the 69th RILEM Week*. Melbourne, Australia: Concrete Institute of Australia.

19. Soroushian, P., K. Ostowari, A. Nossoni, and H. Chowdhury. 2001. "Repair and Strengthening of Concrete Structures through Application of Corrective Posttensioning Forces with Shape Memory Alloys." *Transportation Research Record* 1770: 20–26.

20. Rojob, H., and R. El-Hacha. 2018. "Performance of RC Beams Strengthened with Self-prestressed Fe-SMA Bars Exposed to Freeze-Thaw Cycles and Sustained Load." *Engineering Structures* 169: 107–118.

21. Rojob, H., and R. El-Hacha. 2018. "Fatigue Performance of RC Beams Strengthened with Self-prestressed Iron-Based Shape Memory Alloys." *Engineering Structures* 168: 35–43.

22. Shahverdi, M., C. Czaderski, and M. Motavalli. 2016. "Iron-Based Shape Memory Alloys for Prestressed Near-Surface Mounted Strengthening of Reinforced Concrete Beams." *Construction and Building Materials* 112: 28–38.

23. Shahverdi, M., C. Czaderski, P. Annen, and M. Motavalli. 2016. "Strengthening of RC Beams by Iron-Based Shape Memory Alloy Bars Embedded in a Shotcrete Layer." *Engineering Structures* 117: 263–273.

24. CSA (Canadian Standards Association). 2004. *Concrete Materials and Methods of Concrete Construction/ Methods of Test and Standard Practices for Concrete*. CSA-A23.1-04. Toronto, ON, Canada: CSA Group.

25. ASTM Subcommittee A01.13. 2014. *Standard Test Methods and Definitions for Mechanical Testing of Steel Products*. ASTM A370. West Conshohocken, PA: ASTM International.

26. El-Hacha, R., and M. Gaafar. 2011. "Flexural Strengthening of Reinforced Concrete Beams Using Prestressed, Near-Surface-Mounted CFRP Bars." *PCI Journal* 56 (4): 134–151.

Notation

A_f = austenite finish temperature

A_g = gross area of the beam cross section

A_s = austenite start temperature

e = eccentricity of the Fe-SMA strips

E_c = modulus of elasticity of concrete

f'_c = compressive strength of concrete

I_g = moment of inertia of the beam cross section

L = length

M_f = martensite finish temperature

M_s = martensite start temperature

P = prestressing force in the Fe-SMA strips

P_{cr} = cracking load

P_u = ultimate load

P_y = yielding load

y = distance from the center of gravity of the tension steel to the center of gravity of the beam's cross section

$\Delta\%$ = difference

Δ_u = deflection at ultimate

Δ_y = deflection at yield

ε_c = strain in the concrete at the level of the tension

σ_f = stress level at which detwinning finishes

σ_s = stress level at which detwinning starts

About the authors

Hothifa Rojob received his PhD in 2017 from the University of Calgary in Canada, researching the use of shape-memory alloys in strengthening reinforced concrete members. He is a bridge engineer at Parsons Inc. in Calgary.

Raafat El-Hacha is a Killam Professor and professor of structural engineering at the University of Calgary in the Department of Civil Engineering at the Schulich School of Engineering. His research focuses on using high-performance advanced materials, such as fiber-reinforced polymers, shape-memory alloys, and ultra-high-performance concrete for hybrid structural systems in bridge applications and other structures.

Abstract

An experimental program was conducted to investigate the performance of large-scale reinforced concrete beams strengthened with near-surface-mounted iron-based shape-memory alloy (Fe-SMA) strips. Shape-memory alloys are a unique class of alloys with the ability to undergo large deformations and return to their original shape through stress removal by unloading or heating. Four beams were tested in total, including a control beam and three beams strengthened with near-surface-mounted Fe-SMA strips. One beam was strengthened with five nonactivated strips, and two beams were strengthened with five and seven activated Fe-SMA strips, respectively.

The results revealed the effectiveness of the strengthening technique in enhancing the flexural performance of the strengthened beams at the service and ultimate load conditions. Furthermore, the strengthened beams failed in a ductile failure mode by crushing of concrete after yielding of the steel reinforcements and the Fe-SMA strips, similar to the behavior of an underreinforced concrete beam. The performance of the strengthened beams was compared with similar beams strengthened with prestressed, near-surface-mounted carbon-fiber-reinforced polymer (CFRP) bars with comparable prestressing forces. The comparison revealed the superiority of the near-surface-mounted Fe-SMA in maintaining the ductile behavior of the beams compared with the brittle failure of near-surface-mounted CFRP-strengthened beams.

Keywords

Fe-SMA, iron-based shape-memory alloy, rehabilitation, self-prestressing, shape-memory effect, SMA, SMA strip, strengthening.

Review policy

This paper was reviewed in accordance with the Precast/Prestressed Concrete Institute's peer-review process.

Reader comments

Please address any reader comments to *PCI Journal* editor-in-chief Emily Lorenz at elorenz@pci.org or Precast/Prestressed Concrete Institute, c/o *PCI Journal,* 200 W. Adams St., Suite 2100, Chicago, IL 60606.